UC Santa Barbara
UC Santa Barbara Previously Published Works

Title
Local, Real-Time Measurement of Drying Films of Aqueous Polymer Solutions Using Active Microrheology

Permalink
https://escholarship.org/uc/item/9hf243bn

Journal
Langmuir, 30(18)

ISSN
0743-7463

Authors
Komoda, Yoshiyuki
Leal, L Gary
Squires, Todd M

Publication Date
2014-05-13

DOI
10.1021/la5001733

Peer reviewed

eScholarship.org Powered by the California Digital Library
University of California

Langmuir

Article

pubs.acs.org/Langmuir

Local, Real-Time Measurement of Drying Films of Aqueous Polymer Solutions Using Active Microrheology

Yoshiyuki Komoda,*[†,‡,§] L. Gary Leal,[‡] and Todd M. Squires[‡]

[†]Department of Chemical Science and Engineering, Kobe University, Kobe, Hyogo 657-8501, Japan

[‡]Department of Chemical Engineering, University of California, Santa Barbara, California 93106, United States

ABSTRACT: Oscillatory microdisk rheometry was applied to evaluate the evolution of the viscoelastic properties at the surface of a film of an aqueous solution of poly(vinyl alcohol) (PVA) during drying. The drying rate was measured concurrently, based upon measurements of the variation of film thickness. A fully hydrolyzed PVA solution shows a constant drying rate, while a less hydrolyzed PVA solution exhibits a decreased drying rate in the latter part of the drying process, which occurred at the same time as an increase of the elastic modulus. We suggest that this difference in behavior is a consequence of the fact that both the configuration of the PVA molecule and the strength of interaction with water depend on the degree to which the PVA is hydrolyzed. The polymer concentration at the film surface can be estimated from the measured viscosity at the surface for the fully hydrolyzed PVA solution, and this result then can be compared with two theoretical calculations: one in which the polymer concentration is assumed to remain uniform throughout the film, and the other in which the polymer concentration distribution is determined via a one-dimensional diffusion model. This comparison suggests that the polymer is first concentrated locally near the surface but later in the drying process the distribution of polymer becomes increasingly uniform, possibly due to a spontaneously generated convective flow inside the film.

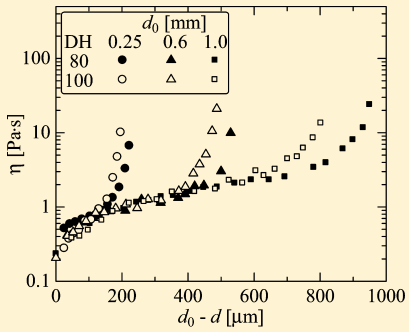

INTRODUCTION

In the drying of thin films of polymer solutions, a solvent evaporates from the drying interface, forming a nonuniform polymer concentration normal to the interface. The evaporation process is governed by the diffusivity of the solvent in the polymer solution and by the gas−liquid equilibrium at the drying interface. As a consequence, many studies have been undertaken to measure and predict the mutual diffusion coefficient over a wide range of polymer concentrations. Okazaki et al. measured the mutual diffusivity and proposed a model of thin film drying.[1] A few years later, Vrentas and Duda described theoretical methods for estimating the mutual diffusion coefficient for infinitely dilute, dilute, and concentrated solutions.[2] Their methods were subsequently applied to simulate the drying process in an industrial dryer by Price and Cairncross[3] and Ramesh and Duda.[4]

Although interactions between polymer molecules are negligible in dilute polymer solutions, hydrodynamic interactions and/or intermolecular associations can play a dominant and controlling role in the diffusion processes during film drying, and this is enhanced due to microstructural rearrangements as the polymer concentration increases during the drying process. Additionally, the increasing polymer concentration causes the viscosity of the polymer solution to increase and sometimes introduces elasticity. Finally, if the drying rate is very large, the drying interface can itself become highly elastic (called "skinning") after which the evaporation rate is sharply reduced. Even if this strong skinning effect is avoided, for example, by reducing the drying rate, an increase in the polymer concentration at or near the surface cannot be avoided, except at infinitely low drying rates.

The rheological properties of the interfacial region reflect the increase in polymer concentration and can therefore provide important information about the dynamics of the drying process. Within the past decade, techniques in microrheology have been used to probe drying films.[5] Kang et al. determined the local polymer solution viscosity from the Brownian motion of a fluorescent tracer particle.[6] Song et al. evaluated the evolution of paint viscosity by measuring the translational velocity of magnetic particles under an applied magnetic field.[7] Additionally, optical tweezers,[8] electric field tweezers,[9] and oscillatory ferromagnetic microbuttons[10] have been utilized as alternative, in situ tools to characterize the microrheological properties of complex fluids, both in the bulk and at interfaces. Among these methods, the oscillatory microbutton holds several advantages for the study of drying processes. A relatively large torque can be applied to the button, enabling measurements of even highly viscous and elastic materials. Furthermore, since the amphiphilic nature of the microbuttons keeps them on the interface as the film dries, the evolution of the fluid viscosity and elasticity near the surface can be measured over a wide range of film thicknesses and drying conditions. Finally, the microbutton provides an effective marker for the position of

Received: January 16, 2014
Revised: April 11, 2014
Published: April 11, 2014

 © 2014 American Chemical Society dx.doi.org/10.1021/la5001733 | *Langmuir* 2014, 30, 5230−5237

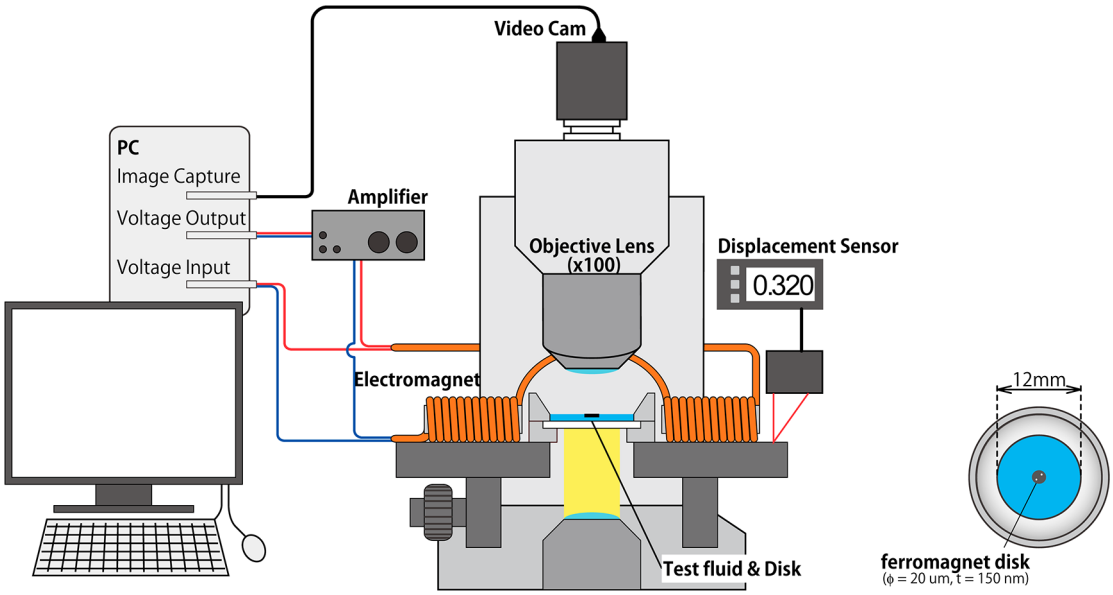

Figure 1. Experimental overview: A PC generates a sinusoidal voltage and records the amplified voltage. Electromagnets establish a sinusoidal magnetic field in response to the ac current, which torques a ferromagnetic microbutton pinned at the interface of the drying fluid. The orientation of the oscillating microbutton on the fluid surface is captured using a CCD video camera and processed using the same PC. As the film dries, the microbutton is kept in focus by adjusting the height of the microscope stage, which is continuously measured by a displacement sensor to determine the film thickness variation.

the drying surface and thus a convenient basis to measure changes in the film thickness.

The objective of the present study is to use the oscillatory ferromagnetic microdisk to clarify the evaporation process of a drying polymer solution based upon the viscosity change in the immediate vicinity of the surface, and the vertical position of the disk as a measure of the film thickness (i.e., the drying rate). We also have discussed the polymer concentration profile estimated from measured viscosities by comparing with theoretical approaches.

■ EXPERIMENTAL SETUP

The experimental setup is composed of an optical microscope with a video camera, a pair of electromagnets surrounding a test cell to hold the thin film, and a laser displacement sensor (Figure 1). The test cell is cylindrical (12 mm in diameter and 1 mm in depth) with a glass bottom, housed between two orthogonal pairs of electromagnets, and placed directly on the microscope stage. The test cell was initially filled with test fluid to a depth 1 mm or less, ensuring the fluid film had a shallow aspect ratio and stayed flat in the central region away from the side walls.

Microbuttons for active microrheology were fabricated photolithography following Choi et al.,[11] with an outer diameter of 20 μm, an overall thickness 1 μm, and a 150 nm thick ferromagnetic layer of nickel, which imparts a ferromagnetic moment in the plane of the microbutton (and thus the interface). To place microbuttons on the interface of test fluid, Choi et al.[10] micropipet a few microliters of microdisk solution gently onto the surface of the test fluid. In the present system, however, this procedure would result in excessive dilution of the test fluid. Instead, a bubble was generated at the tip of the needle syringe, such that the microbutton solution occupied the relatively small volume in the bubble walls. This bubble was then brought into contact with the fluid.

A sinusoidal voltage generated by amplifying the signal from a D/A converter card was applied to the pair of electromagnets, driving a magnetic field of known magnitude and direction, with frequencies between 0.6 and 16.1 Hz. All results below were obtained at 1.1 Hz, unless otherwise specified. Since the magnetic microbutton is designed with two marker holes, its orientation can be precisely analyzed in real time using an image capture card and a custom image processing program written in LabView.[10] The applied voltage and the rotational motion of the button were thus simultaneously measured, and the viscoelastic properties were calculated using eqs 1−3, which will be discussed shortly.

With microbuttons on the interface, the thickness of the film can be determined. The location of the top surface is continuously determined by keeping the button in clear focus, and the relative translation of the stage is measured with a laser displacement sensor with the spatial resolution of 0.1 μm. The film thickness, $d(t)$, is then given by the difference between the initial thickness and the stage translation during drying. Each microrheological measurement requires approximately 1 min, and the film thickness was measured immediately after each rheological measurement. These measurements were repeated at intervals of 5−20 min, depending on the rate of variation of the rheological values or the film thickness.

The temperature in the laboratory was roughly constant at 22 ± 1 °C, and although the humidity of the air surrounding the experimental setup was not controlled, the rate of film shrinkage was roughly constant, ranging from 4 to 7 μm/min. In order to minimize the effect of air flow in the lab, the cell was covered by a plastic shield.

Oscillatory Microdisk Rheometry. In general, the hydrodynamic drag on a disk rotating in a bulk fluid comes from the side, top, and bottom surfaces. If the disk straddles an interface and the drag on the side surface is large compared to that on the top and bottom, the disk motion is dominated by the rheology at the interface itself. This case corresponds to a large Boussinesq number ($Bo = \eta_{\mathrm{interface}}/(\eta_{\mathrm{bulk}} \cdot a)$ where a is the disk radius). On the other hand, if the fluid is homogeneous on the scale of the disk and the disk is sufficiently thin, most of the drag comes from the top and bottom surfaces. In this work, since the magnetic microbutton is pinned on the drying interface and there is no structure at the interface that distinguishes it from the bulk fluid in the film, the drag from the side is negligible ($Bo \ll 1$). The measured rotational drag thus reflects the rheological properties of the fluid below the drying surface and immediately below the disk in a region having a characteristic thickness equivalent to the disk diameter.

The method used to calculate rheological properties is briefly explained here. A uniform magnetic field, oriented perpendicular to the magnetic moment of the disk, oscillates sinusoidally in time

dx.doi.org/10.1021/la5001733 | Langmuir 2014, 30, 5230−5237

according to $B = B_0 e^{i\omega t}$. The torque exerted on the microbutton is given by the vector product of the magnetic field $\boldsymbol{B}(t)$ and the magnetic moment $\boldsymbol{m}$ of the disk. $\boldsymbol{B}$ is imposed nearly in the direction approximately perpendicular to $\boldsymbol{m}$; the torque L is given approximately $L \approx |\boldsymbol{B}||\boldsymbol{m}| \approx L_0 e^{i\omega t}$. The orientation of the microbutton, measured by an angle $\theta(t)$, thus executes oscillatory rotations according to $\theta(t) = \theta_0 e^{i(\omega t+\delta)}$. The relationship between the rotational amplitude and the imposed torque is given by the rotational drag on an infinitely thin disk, half-submerged in a fluid,[12] the fluid flow for which decays like r^{-2} over a characteristic distance given by the radius of the disk. By assuming small amplitude displacements and homogeneous solution rheology in the vicinity of the microbutton, the relationship is $L = (4\pi a^3\eta)\theta_0 e^{i\delta}$, where η is the viscosity at frequency ω. The storage and loss moduli (G' and G'') and the viscosity (η) can be determined from experimental measurements of the oscillation amplitude θ_0 and the phase lag δ according to

$$G' = \frac{mB_0 \cos\delta}{\theta_0 4\pi a^3} \tag{1}$$

$$G'' = \frac{mB_0 \sin\delta}{\theta_0 4\pi a^3} \tag{2}$$

$$\eta = \frac{mB_0 \sin\delta}{\theta_0 4\pi a^3 \omega} \tag{3}$$

These equations are valid if the shear flow produced by the disk motion decays over a distance that is short compared to the depth of the fluid film. At the relatively low frequencies that characterize this experiment, the velocity fields decay over a distance on the order of the disk radius (here 10 μm). In all experiments presented here, the film thicknesses exceed the disk radius at least 3-fold but usually much more, supporting the simple interpretation of the measurement inherent in eqs 1−3.

■ MATERIALS

We prepared aqueous solutions of poly(vinyl alcohol) (PVA) as test fluids. In this work, two kinds of PVA supplied by Kuraray Co., Ltd., Japan were used. The two PVA samples have the same degree of polymerization, 2400, but a different degree of hydrolysis (DH). One is fully hydrolyzed, having very few acetate side groups, denoted by DH = 100, and the other is less hydrolyzed, having 80% hydroxyl and 20% acetate side groups (DH = 80). The molecular weights of the two PVA samples are 106k (DH = 100) and 128k (DH = 80). The concentrations of the PVA solutions are 6 wt % for DH = 100 and 5.5 wt % for DH = 80, so that the solutions have approximately the same zero shear viscosity (Figure 3).

Although water is not an extremely good solvent for PVA, weak hydrogen bonding between the water molecule and the hydroxyl groups of the PVA does lead to dissolution. However, the intramolecular hydrogen bonding is much stronger than the molecular interaction with the solvent, and the conformation of fully hydrolyzed PVA (DH = 100) is therefore more compact (i.e., has a smaller radius of gyration) than the DH = 80 sample. Hong et al. also reported that fully hydrolyzed PVA in water has a very small excluded volume due to strong intramolecular hydrogen bonding.[13] On the other hand, the large number of acetate groups contained in the less hydrolyzed PVA weakens the inter/intra hydrogen bonding, and this leads to a more expanded than the fully hydrolyzed DH = 100 PVA.

■ RESULTS AND DISCUSSION

Accuracy and Validation of Measurement. Although the microbutton was originally developed for interfacial rheology, in this work, we are using it to measure the rheology of bulk solutions. We thus first calibrate the microrheometer by measuring simple Newtonian silicon oils of known viscosity. As expected, Figure 2a shows the measured viscosity to be constant over the range of frequencies investigated. Figure 2b shows excellent agreement between the measured viscosities and the known viscosities of the silicon oils, thus confirming the accuracy of the microbutton rheometry technique for bulk materials. Additionally, the elastic (storage) modulus G', which should be zero, was at least 6 times smaller than the loss modulus G''. The nonzero "measured" value of G' reflects uncertainties of order 5 degrees in the measurement of the phase lag δ. The magnitude $|G^*| = (G'^2 + G''^2)^{1/2}$ is well captured, and the subdominant modulus can be measured to within 10% of the dominant modulus, corresponding to a phase angle (δ) ranging from 6° to 84°.

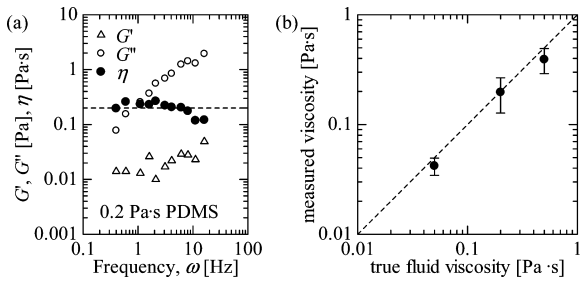

Figure 2. Calibration of oscillatory microdisk rheometry with three silicon oils of viscosity 0.05, 0.2, and 0.5 Pa·s. (a) Frequency-dependent viscoelastic properties of silicon oil (η = 0.2 Pa·s); (b) comparison of viscosity measured microrheologically with the supplier's value.

We now discuss the rheological properties of the PVA solutions. In order to avoid solvent evaporation during these measurements, a small amount of low viscosity silicon oil (3 mPa·s) was spread over the PVA solution film after putting the magnetic microbutton on the PVA surface. The thickness of this film was approximately 50 μm and was thick enough compared with the microbutton diameter that the flow in the oil can be approximated as that in a semi-infinite fluid. The flows in the oil and PVA solution contribute a drag on the bottom (from the PVA solution) and top (from the oil) of the disk that can be expressed as $4\pi\eta_{\text{solution}}a^3$ and $4\pi\eta_{\text{oil}}a^3$. Since the measured resistance is the sum of these contributions, the calculated viscosity from eq 3 is the sum of the viscosities of the PVA solution and oil. The PVA viscosity was then obtained by subtracting the silicon oil viscosity from this calculated viscosity.

Figure 3 shows the viscosity of the fully hydrolyzed PVA solution to be constant for frequencies between 0.5 and 10 Hz, with very small storage moduli. The less hydrolyzed PVA shows a weak (∼30%) frequency-thinning viscosity and larger relative values of G'. The constant viscosity of the fully hydrolyzed PVA solution was consistent with measurements performed with a commercial viscometer. While the Cox−Merz relationship often leads one to expect the shear-rate dependence of the viscosity measured under steady shear to correspond to the frequency dependence of small-amplitude linear oscillatory measurements, the Cox−Merz relationship is based on empirical observations and is well known to not hold universally. The low-shear/low-frequency limits agree quantitatively, as they should, validating the microbutton technique.

dx.doi.org/10.1021/la5001733 | Langmuir 2014, 30, 5230−5237

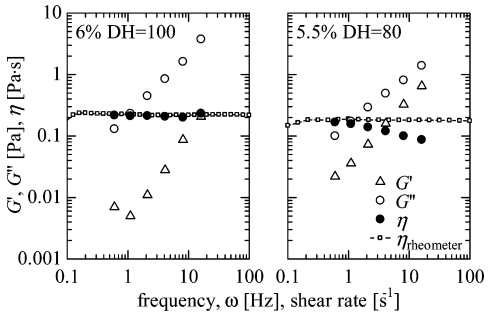

Figure 3. Rheological characterization of PVA solutions. In all cases, the low-frequency viscosity η measured with the microbutton agrees well with the low-shear viscosity $\eta_{rheometer}$, measured by a commercial viscometer. The microbutton shows a slight (~30%) frequency thinning for the DH = 80 solution, for which no corresponding shear thinning is detected by the viscometer. Excellent agreement is found for the 1 Hz measurements used throughout this work.

Variation of Rheological Properties during Drying. Having demonstrated the accuracy of the microdisk rheometer and the rheology of the initial PVA solutions, we now describe measurements during drying of the PVA solution films. Figure 4 shows the evolution of the local rheological properties of the solution near the interface as the solution dries, as well as the film thickness versus time, for both the fully and less hydrolyzed PVA solutions. The results for two initial film thicknesses are shown for each PVA solution. In the early part of the drying process, both G' and G'' increased gradually, while the film thickness decreased at a constant rate (constant drying rate period) for both PVA solutions. The drying rate for the DH = 100 solutions stays constant at 5 μm/min, whereas the average drying rate of the DH = 80 solution ranged from 2.5 to 6.5 μm/min, with a 4 μm/min average rate. Furthermore, G' is consistently smaller for DH = 80 than for DH = 100. Both of these observations are consistent with the expectation that DH = 100 molecules occupy smaller volume, thus providing higher diffusional mobility and weaker elasticity.

However, interesting differences between the PVA solutions appear in the latter part of the drying process. First, the drying rate for the fully hydrolyzed DH = 100 PVA decreases appreciably once the film has decreased to approximately one-third of its initial thickness, whereas the drying rate for the DH = 80 solution remains much more steady throughout the drying process, with only a very slight decrease as the film dries. Second, the elastic modulus G' for the DH = 100 solution begins to increase rapidly at the same time that the drying rate begins to decrease. Since the storage modulus G'' simultaneously shows a rapid (albeit relatively weak) increase, the modulus ratio G''/G' (or loss tangent) decreases. This quantitative shifts in both the drying rate and the storage modulus for the fully hydrolyzed PVA solution suggests qualitative changes to the solution itself in the vicinity of the drying interface. Such rheological changes would be expected, for example, if the (more concentrated) DH = 100 chains in the more dried solution were to interact as strongly as the DH = 80 chains do initially.

The transition from a constant drying rate period to a falling drying rate period for DH = 100 solution may be explained by a change in the rate-limiting mass transport process during

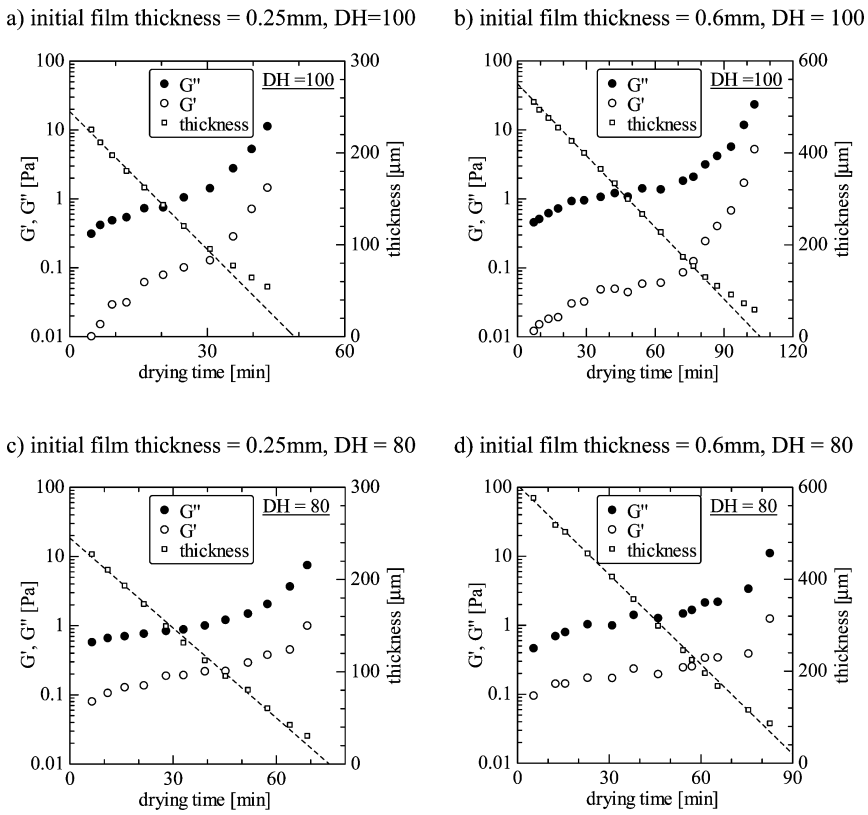

Figure 4. Variation of viscoelastic properties at the frequency of 1.1 Hz and film thickness during drying: The drying rate is initially constant (dashed lines) for all film thicknesses and DH values. Drying rate for DH = 100 solutions decreases slightly in the latter part of the drying process, at which point the measured elastic moduli G' increase simultaneously. Trends for DH = 80 solutions are similar but much weaker.

dx.doi.org/10.1021/la5001733 | Langmuir 2014, 30, 5230−5237

drying. Initial evaporative fluxes are limited by the mass transport resistance of the evaporative flux at the solution/gas interface, which is eventually exceeded by the mass transport resistance of water diffusing within the thin film. Before drying, Hong et al. reported that each fully hydrolyzed PVA molecule forms a tightly aggregated structure due to intramolecular hydrogen bonding, resulting in a solution with little to no elasticity.[13] However, as drying proceeds, the intermolecular separation becomes small enough that the hydrogen bonding between PVA molecules may become significant. In any case, an increased fraction of the remaining water molecules are also associated via molecular bonding with the polymer, which may decrease the average water mobility enough to affect the transport of water to the interface. We thus suggest that association between PVA aggregates increases G' and the arrested water decreases the drying rate. In effect, the PVA concentration in the DH = 100 solutions must be significantly increased (i.e., by the drying process) before the DH = 100 solution exhibits drying rates and elastic moduli that are similar to those of DH = 80.

By contrast, the less hydrolyzed (DH = 80) PVA molecules interact with each other even before the solution has dried, giving elastic moduli G' that are larger than for DH = 100 PVA solutions and drying rates that are slower. Increasing the polymer concentration in the DH = 80 case does not seem to produce a qualitative structural change. Furthermore, interaction between the partially hydrolyzed PVA and the water molecules are weaker than for DH = 100 molecules. Consequently, although G' and G'' increase with time during evaporation, their similar trends with time indicate that no drastic change occurs in either the hydrodynamic interaction or water diffusivity.

Evolution of Concentration Distribution. To access these interpretations, we now examine the drying process from the perspective of water transport. The small aspect ratio of the film suggests a one-dimensional (1D) approximation. Water evaporates from the surface, causing a local increase in polymer concentration near the surface, which attempts to equilibrate with the rest of the film via diffusion. Depending on the relative rates of diffusion and evaporation, the polymer concentration near the surface may increase. Even if the solution were to remain homogeneous (i.e., no concentration gradient was established within the film), the viscosity would increase continuously as the film dries. For homogeneous polymer concentration profiles, however, the drying process should initially be unencumbered by the polymer and then slow down as the polymer concentration increases, with a rate dependence that is reflected in the measured viscosity of the fluid in the vicinity of the surface. Figure 4 reveals that, for all films, the viscous modulus G'' (which is proportional to the local solution viscosity) increases quickly just after drying starts, increases more slowly for a period, and then, increases more rapidly during the latter stages of drying. The duration of the intermediate (slowly increasing viscosity) period depends upon the initial film thickness: relatively short for 0.25 mm films and long for 0.6 mm films, suggesting this period involves the bulk solution, far from the effects of the top or bottom surfaces. Even films with different DH and initial film thicknesses showed similar behavior during their initial periods (first rapid increase in local solution viscosity), leading us to suggest that the initial period reflects evaporation local to the top surface and relatively independent from the bulk or bottom surface. We therefore plot the viscosities measured for these different films against the decrease in film thickness $[d_0 - d(t)]$ in Figure 5, which collapses the data in the initial and intermediate periods, for different film thicknesses and DH values.

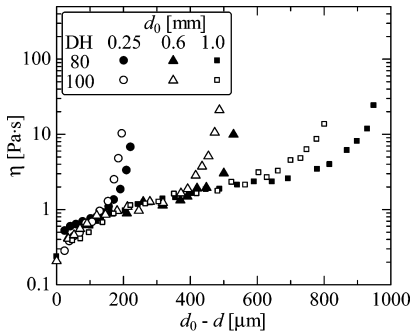

Figure 5. Evolution of viscosity as a function of decrease in thickness (amount of water evaporated), for films with initial thickness d_0 = 0.25, 0.6, and 1.0 mm. The initial viscosity increases correlate with the total decrease in film thickness, regardless of the DH value and initial film thickness, suggesting an initial local concentration of the polymer at the surface. A second rapid increase in viscosity occurs when the film is nearly fully dried (i.e., $d_0 - d$ approaching d_0) and depends strongly upon the DH value, with viscosity increases for fully hydrolyzed PVA occurring earlier than for DH = 80. These observations suggest transitions within the internal, intra-PVA structure as the film is dried enough that the solution becomes strongly concentrated.

The initial increase in viscosity near the interface is largely driven by the amount of water evaporated, rather than the degree of hydrolysis or the initial film thickness. We interpret this to indicate that any decrease in the mobility of water molecules is negligible until the fully hydrolyzed PVA molecules become highly concentrated. Thus, since water molecules can move freely without hydrogen bonding with the PVA molecule in a dilute solution, the initial stage of the drying process is not influenced by the degree of hydrolysis.

After some time, however, a second rapid increase in viscosity is observed, which consistently occurs earlier for the DH = 100 solution than for the DH = 80 solution. At the point where the viscosity shows this second rapid increase, the film has dried to approximately one-third of its initial thickness, corresponding to an average polymer concentration in the film of more than 15 wt % if the polymer solution film is regarded to be homogeneous and with a flat interface. However, the measured viscosities are significantly lower than the O(100 Pa·s) viscosities that would be expected for PVA solutions at these concentrations, as shown in the next section.

Prediction of Polymer Concentration at the Surface. In the following subsections, we discuss three methods to determine the polymer concentration at the surface and then use these predictions to discuss the evaporation process for the polymer film in the final subsection.

Polymer Concentration Determined from the Measured Solution Viscosity. The polymer concentration in the vicinity of the interface can be calculated for the DH = 100 solution from the measured viscosity using the relationship between polymer concentration and solution viscosity provided by the PVA supplier[15] as shown in Figure 6. In the range of polymer concentration ρ_p from 15 to 150 kg/m^3 (1.5−15 wt %) for DH = 100 PVA, the logarithm of polymer concentration is well correlated by a third-order polynomial function of the logarithm of solution viscosity (Figure 6).

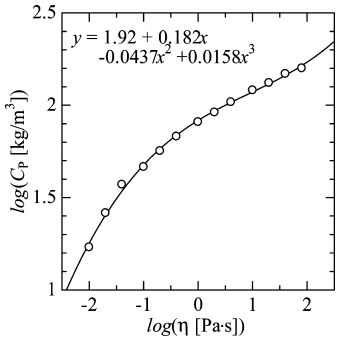

Figure 6. Relationship between polymer concentration and solution viscosity for DH = 100 PVA.

Bounding Polymer Concentration Using Mass Transport Modeling: Quasisteady Concentration of the Solution with Surface Curvature. A lower bound on the polymer solution concentration at the (evaporating) interface can be determined by assuming the polymer to remain fully mixed within the test cell throughout the drying process. Although the test cell is sufficiently wide to form a "nearly" flat surface at the center, we consistently observe menisci near the test cell walls, particularly at the end of the drying process. On the basis of direct measurements of the interface shape with spatial resolutions of 0.5 mm in width and 0.1 μm in height, we therefore make the following approximations for the surface profile: (1) the interface is treated as a half ellipsoid during drying; (2) the contact line is pinned at the cell walls during drying; and (3) the film thickness is measured at the centerline of the cylindrical film, where the thickness is a minimum. A schematic of the surface profile during the drying process appears in Figure 7. Here, D represents the maximum film thickness at the cell wall; d_0 and $d(t)$ represent the minimum film thickness at the center before and during drying.

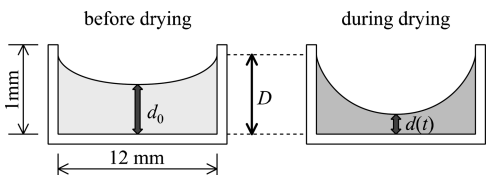

Figure 7. Schematic of the surface profile during drying. We treat the sample/wall contact line as pinned to the wall and the free surface shape as an ellipsoid, based on direct measurements of the interfacial shape. The film thickness $d(t)$ is measured at the center of the test cell.

Then, an equivalent film thickness $X(t)$ can be defined, which is the ratio of total liquid volume to the cross-sectional area of the test cell, and calculated using $X(t) = d(t) + (D - d(t))/3$. Thus, if the polymer were to remain homogeneously distributed throughout the film, the average value of polymer concentration $\rho_p(t)$ (mass/volume) would be given by

$$\rho_{p,avg}(t) = \rho_p(0)X(0)/X(t) \tag{4}$$

If these approximations were correct, the concentration inferred from the viscosity measurements (i.e., Figure 6) would match $\rho_{p,avg}$. This well-mixed limit represents a lower bound on the surface PVA concentration. However, because drying occurs at the upper surface, we expect that the concentration of polymer at that surface will be larger than $\rho_{p,avg}$. We address this issue in the following section.

Modeling 1D Evaporation and Diffusion to Determine the Surface PVA Concentration. As the second limit, we treat the polymer solution as concentrated locally, in the vicinity of the surface, due to the evaporation and resulting diffusion of water and polymer. Since the diffusion coefficient is reduced as the concentration of polymer solution in the solution increases, the diffusion flux should be distributed in the vertical position in the film during drying. The evolution of the water concentration profile has been successfully calculated by Price and Cairncross or Ramesh and Duda for a flat film, based on a 1D diffusion process. The shrinkage of the wet polymer film was explicitly computed by accounting for evaporative mass transfer through the drying interface, and the heat transfer caused by solvent evaporation.

In the present work, however, we explicitly measure the film thickness as a function of time and can therefore seek only to solve determine the polymer concentration distribution without introducing the additional complexities (and uncertainties) involved with the evaporation process itself. We therefore solve directly for the polymer concentration, by assuming that the film is flat enough for a 1D diffusion approximation to be appropriate:

$$\frac{\partial \rho_p}{\partial t} = \frac{\partial}{\partial z}\left(D_m(\rho_p)\frac{\partial \rho_p}{\partial z}\right) \tag{5}$$

where $D_m(\rho_p)$ is the (concentration-dependent) mutual diffusion coefficient.

The measured film thickness $d(t)$ at the center of the film was used to calculate the shrinking rate of equivalent flat film thickness $X(t)$. Since the decreasing rate of measured film thickness is approximately constant, we use a constant rate of equivalent flat film shrinkage to simulate the evaporation process. Boundary and initial conditions appropriate to eq 5 are

$$\begin{aligned} &\rho_p(t = 0, z) = \rho_p^{\,0} \\ &\frac{\partial \rho_p}{\partial z} = 0 \quad \text{at} \quad z = 0 \\ &-D_m\frac{\partial \rho_p}{\partial z} - \rho_p\frac{dX}{dt} = 0 \quad \text{at} \quad z = X(t) \end{aligned} \tag{6}$$

where

$$\frac{dX}{dt} = R(\,=\text{const}) \tag{7}$$

Alternately, one could also impose a conservation equation for the polymer

$$\int_0^{X(t)} \rho_p dz = \text{const} = \int_0^{X(t)} \rho_p^{\,0} dz \tag{8}$$

which is equivalent to (eq 6c).

The domain is shrinking with time. It is convenient to express the problem in terms of a fixed spatial region by scaling with $X(t)$. We first nondimensionalize

$$\bar{\rho}_p = \frac{\rho_p}{\rho_p^{\,0}} \quad \bar{z} = \frac{z}{X(0)} \quad \bar{t} = \frac{D_m^{\,0}}{X(0)^2}t \tag{9}$$

where $X(0)$ is the initial thickness and $D_m^{\,0}$ is the initial mutual diffusion coefficient. The resulting dimensionless equations are

dx.doi.org/10.1021/la5001733 | Langmuir 2014, 30, 5230−5237

$$\frac{\partial \bar{\rho}_p}{\partial \bar{t}} = \frac{\partial}{\partial \bar{z}}\left(Q\frac{\partial \bar{\rho}_p}{\partial \bar{z}}\right) \quad \text{where} \quad Q = \frac{D_m(\bar{\rho}_p)}{D_m(\bar{\rho}_p^0)} = \frac{D_m}{D_m{}^0} \tag{10}$$

with

$$\bar{\rho}_p(\bar{t} = 0, \bar{z}) = 1$$

$$\frac{\partial \bar{\rho}_p}{\partial \bar{z}} = 0 \quad \text{at} \quad \bar{z} = 0 \tag{11}$$

$$-Q\frac{\partial \bar{\rho}_p}{\partial \bar{z}} - \bar{\rho}_p\frac{d\bar{X}}{d\bar{t}} = 0 \quad \text{at} \quad \bar{z} = \bar{X}(\bar{t})$$

Finally, it is convenient to introduce a rescaled variable in place of $\bar{z}$ so that the surface of the film is at a constant value of this new variable:

$$\xi = \frac{\bar{z}}{\bar{X}(\bar{t})} \tag{12}$$

It is important to note that the partial derivative with respect to time at constant $\bar{z}$ is not the same as the derivative with respect to time at the constant. In terms of this new variable, the nondimensionalized equations are

$$\frac{\partial \bar{\rho}_p}{\partial \bar{t}} + \xi\frac{d\bar{X}}{d\bar{t}}\frac{\partial \bar{\rho}_p}{\partial \xi} = \frac{1}{\bar{X}^2}\frac{\partial}{\partial \xi}\left(Q\frac{\partial \bar{\rho}_p}{\partial \xi}\right) \tag{13}$$

with

$$\bar{\rho}_p(\bar{t} = 0, \xi) = 1$$

$$\frac{\partial \bar{\rho}_p}{\partial \xi} = 0 \quad \text{at} \quad \xi = 0 \tag{14}$$

$$-Q\frac{\partial \bar{\rho}_p}{\partial \xi} - \bar{\rho}_p\bar{X}\frac{d\bar{X}}{d\bar{t}} = 0 \quad \text{at} \quad \xi = 1$$

The concentration dependence of the mutual diffusion coefficient D_m (or its nondimensionalized form Q) was determined using a seventh-order polynomial fit to the experimental data due to Okazaki et al.[1] for the fully hydrolyzed PVA−water system. Similar data is not available for the partially hydrolyzed system, and thus, the calculations from this diffusion model were limited to the fully hydrolyzed case. The results from these calculations are reported below.

Discussion on the Polymer Concentration in the Film during Drying Process. As described above, the polymer concentration at the surface of the drying film can be approximated by two different models. A lower bound on the surface concentration is found by assuming the polymer concentration to remain uniform everywhere in the film, as would occur if the solution remains fully mixed during drying. A more accurate approximation accounts explicitly for the diffusive mass transfer, giving the local polymer concentration as a function of position z and time t, using the approach described above.

Viscosities measured at the surface of drying DH = 100 PVA solutions with three different initial film thicknesses (d_0 = 0.25, 0.6, and 1 mm, for which $X(0)$ = 0.50, 0.73, and 1.0 mm) were converted to polymer concentration and shown in Figure 8. Theoretical predictions based on the well-mixed assumption (lower bound, denoted as homogeneous) and the 1D diffusion computations (denoted as 1D diffusion) are shown for comparison. The surface concentrations from the 1D diffusion model qualitatively match the experimental results: the concentration first increases rapidly, then slows, then increases rapidly again once the film has thinned sufficiently. Moreover, the 1D diffusion approximation describes the early stage surface concentration well, whereas both the well-mixed and 1D diffusion approaches give similar predictions in late-stage drying (toward the end of the second rapid increase), in agreement with experiments.

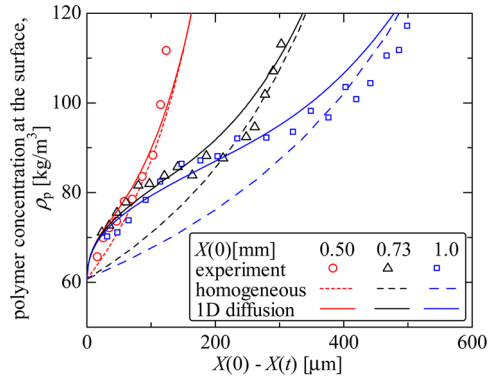

Figure 8. Evolution of the surface concentration of polymer during the drying of DH = 100 films of three different initial thicknesses: d_0 = 0.25 mm ($X(0)$ = 0.5 mm), d_0 = 0.6 mm ($X(0)$ = 0.73 mm), and d_0 = 1 mm ($X(0)$ = 1.0 mm). Notably, the surface concentration during the initial stages of drying are consistent with the nonuniform concentration profiles obtained when the thinning rate is controlled by 1D diffusion. At large times, the fully mixed and 1D diffusion estimates converge, and both match the experimental data.

The surface concentration of the thinnest film (0.5 mm) is well described by either approximation. For the two thicker films, however, the surface concentration initially follows the 1D diffusion model and then appears to shift somewhat toward the well-mixed approximation in the intermediate drying regime. In other words, it appears that the polymer solution is initially concentrated locally at the surface but becomes homogeneous in the latter part of the drying process. Direct observations during drying revealed convective flows directed toward the contact line, leading us to hypothesize that convection may mix and homogenize the concentration. This flow may arise due to Marangoni stresses from nonuniform temperature or polymer concentration profiles along the drying surface or from the convective flows required to conserve mass in a fluid evaporating near a pinned contact line, as occurs in the well-known "coffee-ring" phenomenon.[14] Both of these contributions are intrinsic to the drying process whenever the contact line remains fixed and the film thins faster in the middle than it does in the outer region.

Diffusion coefficients for DH = 80 PVA−water solutions are not currently available, so we did not perform the analogous computations. Nonetheless, we hypothesize that thin film drying follows the same qualitative processes as found for the fully hydrolyzed PVA. Since the less hydrolyzed PVA molecules interact more weakly with water molecules, we expect a higher water diffusivity in DH = 80 PVA solutions than in DH = 100 PVA solutions. This would suggest that more water must evaporate for the DH = 80 PVA solution before the polymer concentrations are homogenized, especially for larger initial thicknesses, leading us to expect higher polymer concentrations at the point of concentration homogenization.

CONCLUSION

We have investigated the drying of thin films of aqueous PVA solutions under moderate drying conditions, by using oscillatory microbutton rheometry to measure the evolution of the rheological properties of the solution near the drying surface, along with the change in film thickness. Two distinct PVA molecules were used, each with different degrees of hydrolysis and hence quite different conformations and different affinities for water. In all cases, we found the viscosity of the PVA solutions near the drying surface initially to increase quickly, then slow, then increase rapidly once again. While both PVA solutions showed similar rheology in the early and middle stages of drying, a difference arose during the final period of rapidly increasing viscosity: the elastic modulus became considerable for the fully hydrolyzed PVA solutions, which was not seen for the less hydrolyzed PVA solutions, and the drying rate decreased. We interpreted the slowing drying rate to reflect the strong interaction between PVA and water molecules.

From known concentration−viscosity relations, we interpreted the local viscosity measurements in terms of polymer concentrations at the surface. We modeled the concentration profiles for DH = 100 solutions whose film thicknesses decreased in a specified manner (i.e., from direct measurements), using both well-mixed and 1D diffusion models. This analysis suggested that inhomogeneous polymer profiles form initially due mass transport limitations of 1D polymer diffusion and were then homogenized (most likely due to convection within the film).

Microbuttons appear particularly well-suited to the measurement of drying films, as they provide real-time, relatively nonperturbative measurements of the local rheology of evolving thin films and coatings.

AUTHOR INFORMATION

Corresponding Author

*E-mail: komoda@kobe-u.ac.jp.

Present Address

[§]Y. Komoda: 1-1, Rokkodai-cho, Nada, Kobe, Hyogo 657-8501, Japan.

Notes

The authors declare no competing financial interest.

REFERENCES

(1) Okazaki, M.; Shioda, K.; Masuda, K.; Toei, R. Drying mechanism of coated film of polymer solution. *J. Chem. Eng. Jpn.* **1974**, *7*, 99−105.

(2) Vrentas, J. S.; Duda, J. L. Molecular diffusion in polymer solution. *J. AIChE* **1979**, *25*, 1−24.

(3) Price, P. E., Jr.; Cairncross, R. A. Optimization of single-zone drying of polymer solution coatings using mathematical modeling. *J. Appl. Polym. Sci.* **2000**, *78*, 149−165.

(4) Ramesh, N.; Duda, J. L. Analysis of a gap dryer used to produce polymer films and coatings. *J. AIChE* **2001**, *47*, 972−983.

(5) Squires, T. M.; Mason, T. G. Fluid mechanics of microrheology. *Annu. Rev. Fluid Mech.* **2010**, *42*, 413−438.

(6) Kang, H.; Ahn, K. H.; Lee, S. J. Rheological properties of dilute polymer solutions determined by particle tracking microrheology and bulk rheology. *Korea-Aust. Rheol. J.* **2010**, *22*, 11−19.

(7) Song, J. O.; Henry, R. M.; Jacobs, R. M.; Francis, L. F. Magnetic microrheometer for in situ characterization of coating viscosity. *Rev. Sci. Instrum.* **2010**, *81*, 093903.

(8) Furst, E. M. Applications of laser tweezers in complex fluid rheology. *Curr. Opin. Colloid Interface Sci.* **2005**, *10*, 79−86.

(9) Sakai, K.; Yamamoto, Y. Electric field tweezers for characterization of liquid surface. *Appl. Phys. Lett.* **2006**, *89*, 211911.

(10) Choi, S. Q.; Jang, S. G.; Pascall, A. J.; Dimitriou, M. D.; Kang, T.; Hawker, C. J. T.; Squires, T. M. Synthesis of multifunctional micrometer-sized particles with magnetic, amphiphilic, and anisotropic properties. *Adv. Mater.* **2011**, *23*, 2348−2352.

(11) Choi, S. Q.; Steltenkamp, S.; Zasadzinski, J. A.; Squires, T. M. Active microrheology and simultaneous visualization of sheared phospholipid monolayers. *Nat. Commun.* **2011**, *2*, 312.

(12) Kim, S.; Karilla, S. *Microhydrodynamics: Principles and Selected Applications*; Butterworths: London, 1991.

(13) Hong, P. D.; Chou, C. M.; He, C. H. Solvent effects on aggregation behavior of polyvinyl alcohol solutions. *Polymer* **2001**, *42*, 6105−6112.

(14) Deegan, R. D.; Bakajin, O.; Dupont, T. F.; Huber, G.; Nagel, S. R.; Witten, T. A. Capillary flow as the cause of ring stains from dried liquid drops. *Nature* **1997**, *389*, 827.

(15) Kurary Webpage. http://www.poval.jp/japan/poval/tec_info/ti_02.html.